Cement and Concrete Composites 90 (2018) 14–26

Contents lists available at ScienceDirect

Cement and Concrete Composites

journal homepage: www.elsevier.com/locate/cemconcomp

Reducing setting time of blended cement paste containing high-SO_3 fly ash (HSFA) using chemical/physical accelerators and by fly ash pre-washing

Franco Zunino [a, *], Dale P. Bentz [b], Javier Castro [c]

[a] Laboratory of Construction Materials, EPFL STI IMX LMC Station 12, CH-1015, Lausanne, Switzerland
[b] National Institute of Standards and Technology, 100 Bureau Drive, Stop 8615, Gaithersburg, MD, 20899, USA
[c] Faculty of Engineering, Universidad del Desarrollo, Chile

ARTICLE INFO

Article history:
Received 19 October 2017
Received in revised form
5 February 2018
Accepted 19 March 2018
Available online 20 March 2018

Keywords:
Sustainability
Hannebachite
Isothermal calorimetry
Supplementary cementitious materials
Hydration kinetics
Flue gas desulphurization (FGD)

ABSTRACT

Reducing the carbon footprint of the cement industry has become one of the main concerns of researchers in the field. This study explores different strategies to reduce the setting retardation effect of high-SO_3 fly ash (HSFA) on cement paste. The SO_3 phase was found to correspond to hannebachite ($CaSO_3 \cdot 0.5H_2O$). Chemical (calcium chloride), physical (fine limestone powder), and pre-washing strategies were investigated as means to reduce or eliminate the retardation. Each of these strategies showed some potential to decrease the retardation effect. A combination of fine limestone powder and HSFA pre-washing showed almost the same accelerating power as the calcium chloride, offering a good alternative when chloride incorporation is restricted. The retardation effect can be associated with a combined extension of the induction period and a depression of the initial silicate reactions of the clinker phases. A methodology to assess the hannebachite content based on a thermogravimetric analysis (TGA) technique is proposed, allowing a good alternative control approach for field conditions or for where X-ray (XRD or XRF) equipment is not readily available.

1. Introduction

Environmental concerns, such as energy consumption and CO_2 emission reductions, have taken special relevance in the construction industry during the last decades [1]. The use of supplementary cementitious materials (SCMs) as a means to reduce the cement content in concrete mixtures [2–4] and enhance the durability of the material and increase the service life of concrete structures [5] has become a topic of increasing interest among researchers.

Fly ash (FA), a by-product of coal combustion in thermal power plants, has been successfully used as an SCM for partial cement replacement [6–13]. The effects and contributions of FA on rheology and setting [9,14], phase assemblage [15,16], strength development [8,14,17], and durability [18–20] have been widely studied.

Some FAs may exhibit a strong retardation effect on the initial setting of cement paste, compromising their feasibility as a cement replacement material, although the interaction mechanism producing the retardation has not been described in detail. Fine limestone powder has been successfully used to accelerate the rate of reaction of cement clinker and partially offset the retardation effect [21], and its efficiency has been also studied in blended FA-limestone systems [15,16,22].

Environmental concerns about coal power plants' flue gas emissions have led to the widespread adoption of desulfurization units, high efficiency burners, and particulate material precipitators [23,24]. While these technologies have indeed exhibited a positive impact on the emissions level and their composition, they can also affect the composition of the FA generated, as some of the residues extracted from the flue gas may be precipitated along with the FA.

This project describes a systematic assessment of the feasibility of using FA that contains sulfur compounds that are combined with the solid phase during precipitation. Stage one is focused on the characterization of the sulfur-rich compounds and their interaction with cement phases at early (from mixing up to 7 d) and later ages. Among the effects at early ages, setting time retardation is a critical

* Corresponding author.
E-mail addresses: franco.zunino@epfl.ch (F. Zunino), dale.bentz@nist.gov (D.P. Bentz), javiercastro@ingenieros.udd.cl (J. Castro).

https://doi.org/10.1016/j.cemconcomp.2018.03.018
0958-9465/

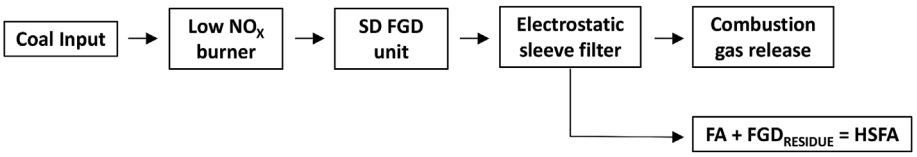

Fig. 1. Schematic diagram of the coal burning unit of the power plants from which the FA considered in this study was collected.

issue that needs to be addressed for a successful use of these FAs. The current study explores several alternatives to offset the observed retardation of initial setting time in cement paste mixtures incorporating these sulfur-rich FAs.

2. High-SO_3 fly ash (HSFA): semi-dry flue gas desulfurization (FGD) process

The pollutants that can be released as a result of combustion in a coal power plant are particulate matter, sulfur dioxide (SO_2), nitrogen oxides (NO_X), carbon monoxide (CO), carbon dioxide (CO_2), unburned hydrocarbons, dioxins, and furans [25]. Several technologies have been developed to reduce the amount of pollutants in the exhaust gas and therefore, comply with the increasingly stricter regulations concerning the environmental impact of these industries.

Regarding the twin power units from which the FA samples were collected for this study, two technological devices were installed to reduce pollutants in the exhaust gas (Fig. 1). First, the use of a low-NO_X coal burner leads to a reduced amount of this pollutant in the gas fraction, with the remaining compounds retained in the solid particles of the combustion flux. Following the combustion stage, a semi-dry flue gas desulfurization (SD-FGD) unit, consisting of a solution of calcium hydroxide ($Ca(OH)_2$), is injected as atomized fine droplets into the flux. Calcium hydroxide combines with the SO_2 in the flue gas, leading to the formation of calcium sulfite ($CaSO_3$) and water. In some plants, a forced oxidizing stage is included after the FGD to transform this calcium sulfite into gypsum ($CaSO_4 \cdot 2H_2O$), which has commercial value. Furthermore, a first sleeve filter is usually placed between the burner and the FGD unit to collect the FA before intermixing with the FGD by-products, especially when this FA is viewed as a valuable by-product itself. However, none of these stages are implemented in the power units considered in this study, consistent with commercial practice at many existing power plants. Because of the joint collection of FA and the by-products of the FGD unit, the obtained FA exhibits high levels of SO_3-rich compounds when it is collected from the power plant.

For the purpose of this study, high-SO_3 fly ash (HSFA) is defined as any FA material with a measured SO_3 content above the maximum of 5.0% prescribed by ASTM C618 [26]. The aim of the inclusion of this restriction in the standard was to limit the amount of gypsum in FA, which can lead to sulfate-related deleterious reactions in concrete [27,28]. However, for a dry or semi-dry FGD process, previous related studies have shown that the formed by-product solid sulfur-rich phase is mainly composed of calcium sulfite ($CaSO_3$) [23,29–31]. Thus, the stability (reactivity) of this compound and difference in its chemical behavior relative to its oxidized form (gypsum), needs to be understood to assess the feasibility of the utilization of HSFA in cement-based materials.

3. Materials and methods

Two different fly ash samples (named FA-1 and FA-2) were selected for this study. Both ashes were obtained from a power plant with the desulfurization process described in the previous section. Because of this FGD scheme, high amounts of sulfur-rich compounds are found in the ashes. The chemical and physical nature of these materials are addressed in the forthcoming sections.

Table 1
Chemical composition of OPC and HSFA samples (mass %) and phase composition of OPC.

	OPC	FA-1	FA-2	LS
SiO_2	21.59	42.04	40.28	–
Al_2O_3	3.82	17.07	16.26	–
Fe_2O_3	3.05	4.58	3.54	–
CaO	64.34	18.08	19.76	–
Na_2O	0.54	0.51	0.42	–
K_2O	0.46	1.32	0.92	–
MnO	0.06	0.05	0.04	–
TiO_2	0.33	0.81	0.84	–
MgO	1.84	1.47	1.20	–
P_2O_5	0.19	0.16	0.14	–
SO_3	2.87	8.65	10.11	–
LOI	1.6	4.9	5.9	–
$SiO_2 + Al_2O_3 + Fe_2O_3$	28.5	63.7	60.1	–
C_3S	68.51	–	–	–
C_2S	11.72	–	–	–
C_3A	6.58	–	–	–
C_4AF	9.83	–	–	–
Sp. gravity (g/cm^3)	3.122	2.117	2.274	2.750
SSA (m^2/g)	1.27	4.12	4.77	1.53

Type I ordinary Portland cement (OPC) was used for the entire experimental program. Chemical compositions of the OPC and HSFA samples were determined by X-ray fluorescence (XRF), and the results are shown in Table 1, along with the phase composition of the OPC as determined by quantitative X-ray diffraction (QXRD). Limestone (LS) powder (calcite) was obtained from a local supplier. The calcium carbonate ($CaCO_3$) content was determined by thermogravimetric analysis, measuring 98%. The specific gravity of the materials was determined using nitrogen pycnometry. The specific surface area (SSA) of the powder materials was determined by gas adsorption using the Brunauer-Emmett-Teller (BET) method, with a Micromeritics TriStar II[1] analyzer. Nitrogen (N_2) was used as the analysis gas.

For the XRF analysis, the fusion beads sample preparation method was used, using lithium tetraborate ($Li_2B_4O_7$) as the fluxing agent. By this method, the compounds in the ashes are oxidized and therefore, no distinction between different oxidation states can be obtained. This implies that the elemental quantification is obtained as an overall value of abundance in the sample, independent of the oxidation state of the actual compounds present. Both HSFA correspond to Class C FA according to the ASTM C618 classification scheme [26]. In addition, the same standard establishes a 5.0% limit for SO_3 content, which is well surpassed for both FA studied (thus corresponding to HSFA based on the definition presented before).

[1] Certain commercial products are identified in this paper to specify the materials used and the procedures employed. In no case does such identification imply endorsement or recommendation by NIST, EPFL or Universidad del Desarrollo, nor does it indicate that the products are necessarily the best available for the purpose.

The spirit of this restriction is to limit the amount of gypsum ($CaSO_4 \cdot 2H_2O$), which in excess can severely affect the hydration of the aluminate phases and generate durability issues [32,33]. However, as will be shown in the subsequent sections, this is not the mineral nature of the sulfur-rich phase present in these HSFAs. XRF measurements conducted over similar materials shows that the standard deviation of the obtained values is below 0.5% for the most abundant oxide (50%–70% by mass).

3.1. Fly ash characterization techniques

3.1.1. X-ray diffraction (XRD)

XRD analysis was performed to determine the mineral composition of the OPC and HSFA samples. The diffraction patterns were acquired on a Bruker D2 Phaser diffractometer equipped with a Cu Kα source working at 30 kV/10 mA, and a solid state LinxEye detector, in the range 10°–90° 2θ (0.71–5.76 $Å^{-1}$), using a step size of 0.01° 2θ, with an equivalent exposure time of 0.5 s per step. Commercial software Match! was used for phase identification, coupled with the PDF2 database.

3.1.2. Thermogravimetric analysis (TGA) – alternative SO_3 content determination

While XRF offers a proven and reliable technique to assess the SO_3 content of HSFA, sample preparation and equipment availability sometimes limit its applicability in all scenarios. Furthermore, XRF cannot distinguish the mineral origin of the measured SO_3. The thermal decomposition of calcium sulfate ($CaSO_4$) and calcium sulfite ($CaSO_3$) hydrated salts are well described and are easily distinguishable by TGA analysis [24,34]. Therefore, separate quantification of both phases can be easily performed using the measured mass loss and the molar masses of the released compound and the original mineral present in the HSFA. The two HSFA samples considered in this study were analyzed between 30 °C and 1000 °C, with a heating rate of 10 °C/min and under a protective nitrogen (N_2) atmosphere flowing at 50 mL/min. About 40 mg of HSFA sample were placed in alumina crucibles without additional grinding.

A previous study used the water release from $CaSO_3 \cdot 0.5H_2O$ (hannebachite) between 300 °C and 370 °C to quantify this compound in several FGD residues [24]. Based on trials with pure hannebachite, the temperature range was adjusted to 300 °C–400 °C in this study to capture more accurately the mass loss associated with dehydration. This mass loss can be used to determine the amount of hannebachite present in the initial sample by a simple mass balance and from there, the equivalent SO_3 content (SO_3-$_{EQTGA}$), using Eq. (1).

$$SO_{3-EQTGA} = \%massloss_{300-400°C} \cdot \frac{Molar\_mass(SO_3)}{0.5 \cdot Molar\_mass(H_2O)} \quad (1)$$

The SO_3s_{EQTGA} content was compared with the SO_3 content measured by XRF for several other HSFA and Class F (SO_3 content below 5.0%) fly ash samples in addition to the ones considered in this study, in order to validate this alternative approach for measuring SO_3 content. In previous studies, it has been observed that the typical uncertainty for quantitative phase analysis using TGA is represented by a coefficient of variation of less than 5% for phase fractions in the range of 2%–15% [10].

3.1.3. Particle size distribution

Particle size distributions (PSD) of HSFA (raw or pre-washed (W)), LS, fine LS (FLS) and OPC were measured using a Malvern Mastersizer 2000 laser diffractometer. Isopropanol (refractive index 1.378) was used as a dispersant, and the PSD was measured for 20 s while stirring at 2700 rpm. For PSD calculations, 1.610/0.1, 1.596/0.001 and 1.700/0.1 were used as refractive index/extinction coefficient (real/imaginary) of the HSFAs, LS, and OPC, respectively [35]. Results are shown in Fig. 2.

3.1.4. Scanning electron microscopy (SEM)

SEM observations were conducted to understand the morphology and elemental distribution of the HSFA samples at a micro scale. For the morphology assessment, a FEI XL series microscope equipped with a field emission tip and an in-lens SE detector was used to perform high resolution imaging (HR-SEM). Each HSFA powder sample (FA-1 and FA-2) was dispersed in a 0.01% sodium poly-acrylic acid solution. A few droplets of the suspension were dispensed and dried on glass plates. Afterwards, the particles were placed over carbon holders and coated with osmium oxide (OsO_4), to avoid interference of the coating crystallites with the morphological features of the ashes at the nanometer scale.

For the elemental distribution mapping, a FEI Quanta 200 SEM equipped with a Bruker XFlash 4030 EDS detector was used. The accelerating voltage was set at 15 kV and the working distance to 12.5 mm. The powder samples were dispersed in a low viscosity epoxy and cured for 24 h at room temperature. Subsequently, the samples were polished down to 1 μm, coated with carbon and mapped in 4 different areas each at 400× magnification. Backscatter electron images and EDS full elemental maps consisting of 4 frames of dimensions 640 μm by 480 μm were collected.

3.2. Setting time acceleration strategies

Initial setting is closely related to hydration kinetics, as it marks the formation of the first percolated structure by interconnection of solid particles and hydration products. Among the strategies for mitigating the retarding influences of SCMs on Portland cement hydration, chemical acceleration using admixtures and physical acceleration using fine mineral additions have been explored in depth [21,36]. In this study, both approaches are explored, plus a novel FA pre-washing procedure. A similar approach is described in work previously patented, where FA is pre-soaked in water to reduce the interference between FA and the normal hydration of cement [37].

3.2.1. Physical acceleration: limestone powder

Limestone (LS) powder was selected as a physical accelerator because its capabilities and potential in this matter have been proven in previous studies [21,38]. The LS powder was characterized and used as received. The same LS powder was additionally ground in a jar mill for 5 d to obtain a finer powder (FLS, with an SSA of 3.60 m^2/g), in order to assess the effect of additional surface on setting time and early-age hydration (see Fig. 2 for PSDs of LS and FLS). Previous studies have shown that increasing the limestone surface area provides a further reduction of the initial setting time of blended OPC-FA systems, reducing setting times of mortars [22], providing additional nucleation sites for hydration (filler effect) [39–41] and also actively taking part in the percolated backbone upon initial setting [38].

3.2.2. Chemical acceleration: calcium chloride

Calcium chloride dihydrate ($CaCl_2 \cdot 2H_2O$) was used as a setting and hydration chemical accelerator. While limiting provisions for using chloride accelerators are prevalent due to durability concerns [42], it was selected for being one of the most inexpensive and widely adopted chemical accelerators, and also for providing comparable setting accelerating power to limestone powder in the ranges explored in this study [21].

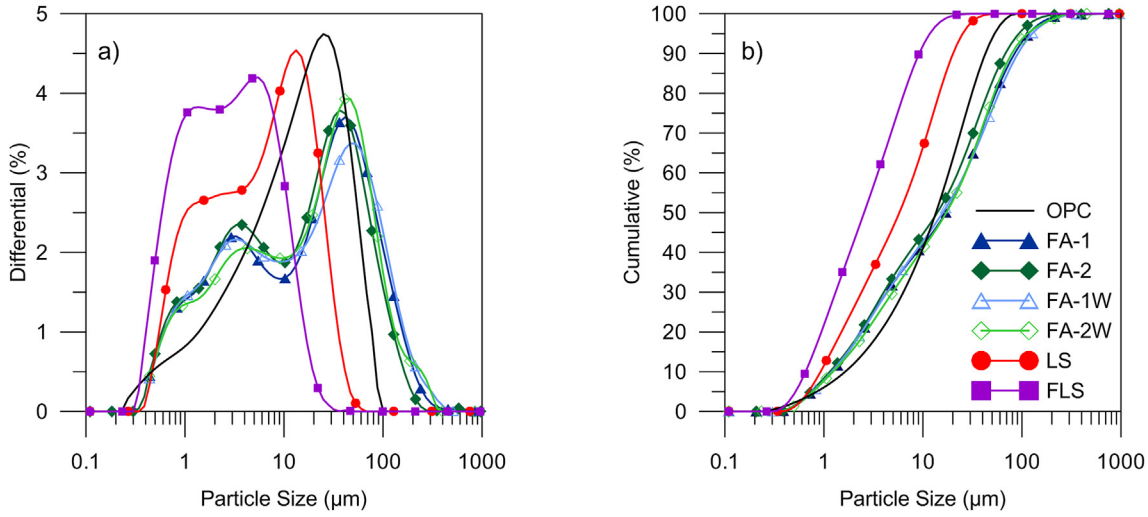

Fig. 2. Particle size distributions (PSD) of the raw materials used in this study, a) differential and b) cumulative plots.

3.2.3. Fly ash pre-washing

For the pre-washing process, 180 g of HSFA were placed over a 0.45 μm filter (100 mm diameter) in a Büchner funnel, and 500 mL of distilled water were passed through the sample under vacuum. After no further washing water was collected in the system, the washed samples (code named FA-1W and FA-2W for washed samples of FA-1 and FA-2, respectively) were placed in an oven and dried at 105 °C for 24 h. PSD and XRD analysis was performed on the washed samples to determine any changes in their particle size distribution due to dilution/non-retention during the process and any variation in their mineralogical composition.

3.3. Setting time and early-age hydration assessment

3.3.1. Vicat setting time test

Setting was measured using an automatic (Vicat) instrument that made needle penetration measurements in fresh locations every 10 min, starting after a user-selected delay. The machine was placed in a temperature controlled room maintained at 23 °C ±3 °C. According to the ASTM C191 test method [43], the single laboratory precision for initial time of setting (taken as the time when a penetration of 25 mm is first achieved) is 12 min.

3.3.2. Isothermal calorimetry

Isothermal calorimetry measurements were conducted using a TAM Air isothermal calorimeter at 23 °C to study the early-age kinetics and hydration development of the mixtures. Tests were conducted on cement paste samples from the same batches as the samples used in compressive strength tests and were kept in the calorimeter up to 3 d. Regarding variability and repeatability of the test, the average absolute difference between replicate specimens was previously measured to be $2.4 \cdot 10^{-5}$ W/g (cement), for measurements conducted between 1 h and 7 d after mixing [9].

3.3.3. Compressive strength

For early-age strength measurements, cubic specimens of paste 20 mm on a side were used. Specimens were removed from their molds after one day of curing and stored in sealed bags in a chamber at 23 °C ± 3 °C and 95% relative humidity (RH) until the time of testing. Compressive strength tests were conducted at 3 d and 7 d on 3 specimens at each age, with a constant 1.8 kN/s loading rate being employed in all cases.

4. Mixture proportions

Mixture proportions were designed on a volumetric basis, maintaining a constant volume fraction of water and solids [10,22]. A 100% OPC mixture with a water-to-cementitious material (*w/cm*) and water-to-solids (*w/s*) ratio by mass of 0.45 was selected as a reference for volume fraction proportioning (*w/s* of 1.405 by volume). This volumetric procedure allows avoidance of the confounding effect of a mass-based replacement between the contributions of the different accelerating strategies, FA reactivity, and initial porosity, given by water volume fraction [10].

In the binary mixtures, the FA replacement level was fixed at 30% by volume of cement, which allowed a clear expression of the FA retarding effect. For the ternary mixtures containing LS or FLS, the replacement was performed over the FA fraction on a 3-to-1 FA to LS (or FLS) ratio by volume [22]. Thus, for a mixture containing 30% by volume of FA, the volume was distributed as 7.5% LS and 22.5% FA. Reagent grade calcium chloride (dihydrate) was added on top of the total mixture, at 1% (only for setting time tests), 2%, and 3% by mass of the cement. Considering its dihydrate form, 75.5% by mass of the salt is calcium chloride. Mixture proportions of the eight mixtures are summarized in Table 2.

5. Results and discussion

5.1. X-ray diffraction (XRD) and thermogravimetric analysis (TGA)

The XRD patterns of the HSFA samples before and after the pre-washing treatment are shown in Fig. 3. Results are presented for qualitative observation of the mineral phases present, despite efforts for quantification through Rietveld refinement being performed. However, it was noted that the crystalline structure of hannebachite ($CaSO_3 \cdot 0.5H_2O$) has been poorly described in the literature compared to those of anhydrite, bassanite, or gypsum ($CaSO_4$, $CaSO_4 \cdot 0.5H_2O$ and $CaSO_4 \cdot 2H_2O$, respectively). In fact, only two published crystalline structures could be found for hannebachite: one by Schropfer in 1973 [44] and the other by Hentschel et al., in 1985 [45]. Neither of these structures appeared to accurately describe the mineral compound found in the ashes, prohibiting a good fit of the model. Consequently, no quantitative information on hannebachite content could be extracted from the results. However, the phase identification does give interesting insights into the effect of the pre-washing treatment on HSFA

Table 2
Mixture proportions used in this study.

MIX ID	Control	FA-1(2)	FA-1(2)W	FA-1(2) + LS	FA-1(2)+FLS	FA-1 + 1%$CaCl_2$	FA-1(2) + 2%$CaCl_2$	FA-1(2) + 3%$CaCl_2$
OPC (vol. %)	100	70	70	70	70	70	70	70
LS or FLS (vol. %)	0	0	0	7.5	7.5	–	–	–
FA-1 (FA-2) (vol. %)	0	30	30	22.5	22.5	30	30	30
OPC (g)	400	280	280	280	280	280	280	280
LS or FLS (g)	0	–	–	26.43	26.43	–	–	–
$CaCl_2 \cdot 2H_2O$ (g)	0	–	–	–	–	2.80	5.60	8.40
FA-1 (FA-2) (g)	0	81.37(87.41)	81.37(87.41)	61.03(65.55)	61.03(65.55)	81.37(87.41)	81.37(87.41)	81.37(87.41)
Water (g)	180	180	180	180	180	180	180	180
Vol. of solids (cm^3)	308.12	308.12	308.12	308.12	308.12	308.12	308.12	308.12
w/s (vol.)	1.405	1.405	1.405	1.405	1.405	1.405	1.405	1.405
w/s (mass)	0.45	0.50(0.49)	0.50(0.49)	0.49(0.48)	0.49(0.48)	0.50(0.49)	0.50(0.49)	0.50(0.49)
w/cm[A] (mass)	0.45	0.50(0.49)	0.50(0.49)	0.53(0.52)	0.53(0.52)	0.50(0.49)	0.50(0.49)	0.50(0.49)

[A]For computing *w/cm* in this study, cement and fly ash are considered as cementitious materials, but not the limestone powder.

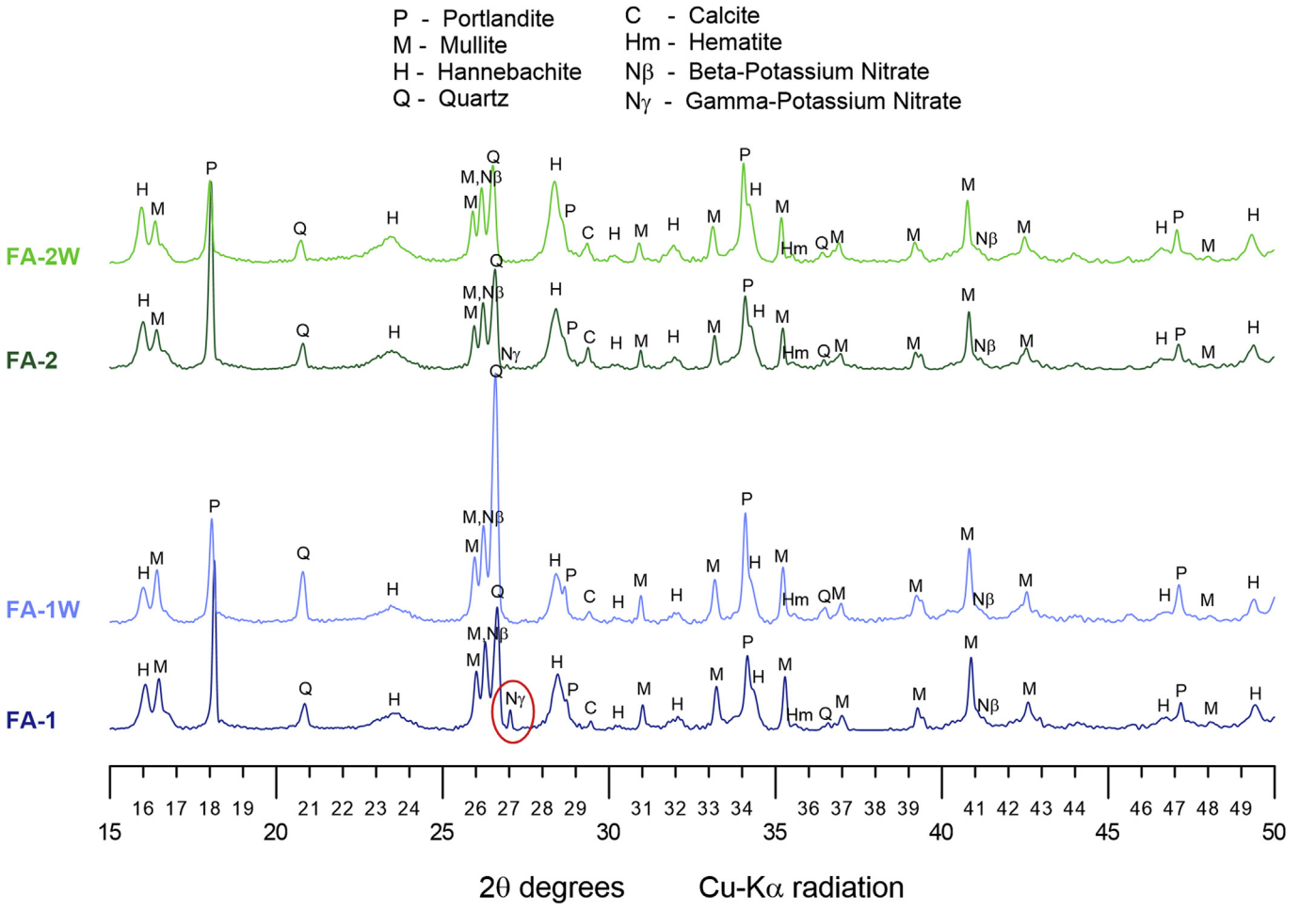

Fig. 3. X-ray diffraction (XRD) patterns for HSFA samples before (FA-1 and FA-2) and after (FA-1W and FA-2W) the pre-washing treatment.

mineralogy.

As observed in Fig. 3, the mineral compositions of both raw HSFA (FA-1 and FA-2) are similar. The presence of typical minerals found in fly ashes such as alumino-siliceous (mullite) and silica (quartz) rich phases are present in both samples. Calcite ($CaCO_3$) and portlandite ($Ca(OH)_2$) are also present, most likely as residues from the combined FGD process involved in these particular power plant units. The hannebachite peaks are clearly identified in both materials, and no traces of calcium sulfate or any of its hydrated forms are observed, in agreement with previous observations concerning semi-dry FGD process solid residues [23,29–31]. Beta and gamma potassium nitrate are observed in both ashes, which is attributed to the use of a low-NO_X coal combustor in both units; reducing the effluent NO_x in the gas could lead to retention of nitrates in the solid residues. After the pre-washing treatment, the amount of potassium nitrate (gamma) is reduced significantly in the ashes (see FA-1W and FA-2W on Fig. 3), due to its high solubility in water. In contrast to the fairly high solubility of gypsum, the

solubility of calcium sulfite is very low in water at ambient temperature, with reported values around $4.5 \cdot 10^{-4}$ mol/dm^3 or in terms of mass, 0.054 g/dm^3 [46], almost 50 times lower than the $1.4 \cdot 10^{-2}$ mol/dm^3 (2.4 g/dm^3) solubility of gypsum [47]. Therefore, one might expect significant calcium sulfite to remain after the pre-washing procedure, with peaks of similar intensities to those observed for untreated samples. The intensity of the (001) portlandite peak also decreased noticeably after the pre-washing procedure. The intensity of the peaks of other phases remained fairly constant, which supports that no particles were lost during the filtration and only soluble compounds were removed/reduced. This is further validated by the barely detectable variation in PSD observed between HSFA samples before and after their pre-washing (Fig. 2).

TGA results are presented in Fig. 4, where the decompositions of interest are marked in the figure for ease of identification.

FA-1 exhibited a mass loss between 300 °C and 400 °C of 1.01%, which can be translated into an 8.83% equivalent SO_3 content by computation using Eq. (1). Similarly, FA-2 exhibited a mass loss of 1.12% in the same temperature range, which corresponds to a 9.96% equivalent SO_3 content. Both values are within 5% of variation of the measured SO_3 content by XRF (see Table 1) and in general the accuracy is within 10% when considering additional HSFA samples to validate the procedure, as shown in Fig. 5. Regarding the pure hannebachite analysis, the decomposition between 300 °C and 400 °C was 6.88% in N_2 and 6.67% in an air atmosphere, which are equivalent to 98.6% and 97.5% initial hannebachite contents, respectively. The decomposition of portlandite (400 °C-500 °C) and the decarbonation of calcite (650 °C-800 °C) are also clearly identifiable in the TGA curves shown in Fig. 4.

In a reducing atmosphere (e.g., N_2) anhydrous $CaSO_3$ decomposes into calcium oxide (CaO), calcium sulfide (CaS), sulfur oxides (SO_x) and oxygen (O_2) between 800 °C and 1000 °C, SO_x being released as a gas and being measured as a mass loss along with oxygen [48]. As seen in Fig. 4, the decomposition over this range for FA-1 and FA-2 also approaches the SO_3 contents determined by XRF (see Table 1), but the measure is less reliable as the proportion between SO_x and O_2 released is unknown. In the case of the pure hannebachite used in this study, the decomposition continued above 1000 °C, thus, the value presented in Fig. 4 considers the mass loss up to 1100 °C. This decomposition does not take place in the presence of oxygen (e.g., in air [49]), where the material undergoes oxidation and transforms into calcium sulfate, which is observed as an overall mass gain of the sample after calcination compared to its initial mass (2.73% for the hannebachite analyzed, which indicates that full oxidation did not occur during the test). On the other hand, the dehydration between 300 °C and 400 °C occurs both in reducing and oxidizing environments. Therefore, the analysis based on this range could be performed by a simple dehydration of the HSFA samples using a common laboratory furnace and a scale, where TGA equipment is not readily available. A source of error of the gravimetric measurement method is the uncertainty of the initial water content of the calcium sulfite compounds. However, the accuracy is at least high enough for quality control and field monitoring purposes.

5.2. Vicat setting time

Setting time results for all of the systems studied are presented in Fig. 6 as needle penetration curves versus time. The FA-1 and FA-2 (30% FA by volume) systems exhibited initial setting times of 12.5 h and 11.8 h respectively, which is equivalent to a retardation of 2.92 (delay of 8.2 h) and 2.76 (delay of 7.5 h) times compared to the reference control mixture (initial setting time equal to 4.3 h). Fig. 6 allows a visual comparison of the effectiveness of the different acceleration strategies explored in this study. The addition of limestone (FA-1+LS and FA-2+LS) produces a reduction of the setting time equivalent to a relative improvement over the FA-1 and FA-2 cases of only 8.4% and 5.5%, respectively. As the limestone addition is refined (FLS), its specific surface area increases and the setting time reduction is significantly improved (21.8% and 21.1% improvement for FA-1 and FA-2, respectively). This can likely be attributed to the additional sites for preferential nucleation of OPC hydration products [21,38,39], which in turn accelerate the formation of the first percolated backbone.

The fly-ash pre-washing treatment proved very effective at mitigating setting time retardation, with observed improvements of 28.0% and 25.6% of FA-1W and FA-2W compared to FA-1 and FA-2, respectively, better than the results observed for the FLS powder. Based on XRD results, pre-washing removes potassium nitrate (KNO_3) from the fly ashes. OPC + KNO_3 mixtures were prepared to verify that this component could explain part of the observed retardation. As seen in Fig. 6, KNO_3 produces a measurable retardation of the initial setting time, increasing it to 5.35 h (a 25% retardation) for an addition of 0.50 g of KNO_3 to a mixture containing 400 g of OPC. This retardation is on the same order as the difference between FA-1W/FA-1 and FA-2W/FA-2 (38% and 34% of the delay, respectively of the un-washed FA mixture referred to the pre-washed case). Thus, the removal of nitrate-rich phases from the HSFA seems to explain much of the improvement observed after pre-washing. A combination of FA pre-washing and physical acceleration was also explored (FA-1W + FLS), with a measured initial setting time of 7.9 h. This represents a retardation of 84% over the Control or a 108% improvement compared to the FA-1 case (retardation of 192% over Control), at the same clinker factor.

Calcium chloride also proved to be effective in reducing the initial setting time, by accelerating the hydration of the silicate phases in OPC, especially C_3S [36,50]. With a 3% $CaCl_2$ addition, the setting time delays are reduced to 47.6% and 45.9% for FA-1 and FA-2, respectively, thus qualifying as the most effective strategy considered. However, this high amount of calcium chloride is usually not permitted by codes for reinforced concrete elements, due to the increased risk of rebar corrosion [42].

5.3. Compressive strength

Compressive strength measurements of cement paste cubes are presented in Table 3. At 3 d, all of the modified mixtures exhibited slightly increased strengths in comparison to their corresponding base blended FA-1 and FA-2 systems. Strength improvement is expected because physical and chemical acceleration strategies seek to accelerate the hydration of OPC and, therefore, the formation of C-S-H. On the other hand, FA pre-washing provides a reduction in the retarding effect of HSFA on the hydration of the silicate phases of the cement. The enhancing effect on strength is more clearly observed at 7 d. No significant difference between LS and FLS is observed at 3 d. This is attributed to the relatively small amount of limestone in the mixtures, which may dilute the differences observed when increasing the specific surface of the limestone. Differences observed in setting behavior may correspond to strength differences among FLS systems before 3 d, as will be shown in the next section. After 3 d, strength development is dominated by the ongoing hydration of cement and the formation of CO_3-AFm phases (hemi and monocarboaluminate) from the reaction of limestone with aluminates. While a finer limestone is expected to react faster, the overall contribution of these phases to space filling and strength is rather small [51], and its reactivity is limited to the available aluminates sourced from the OPC [52,53].

At 7 d, mixtures containing $CaCl_2$ had slightly lower strengths compared to mixtures using other strategies. This behavior has

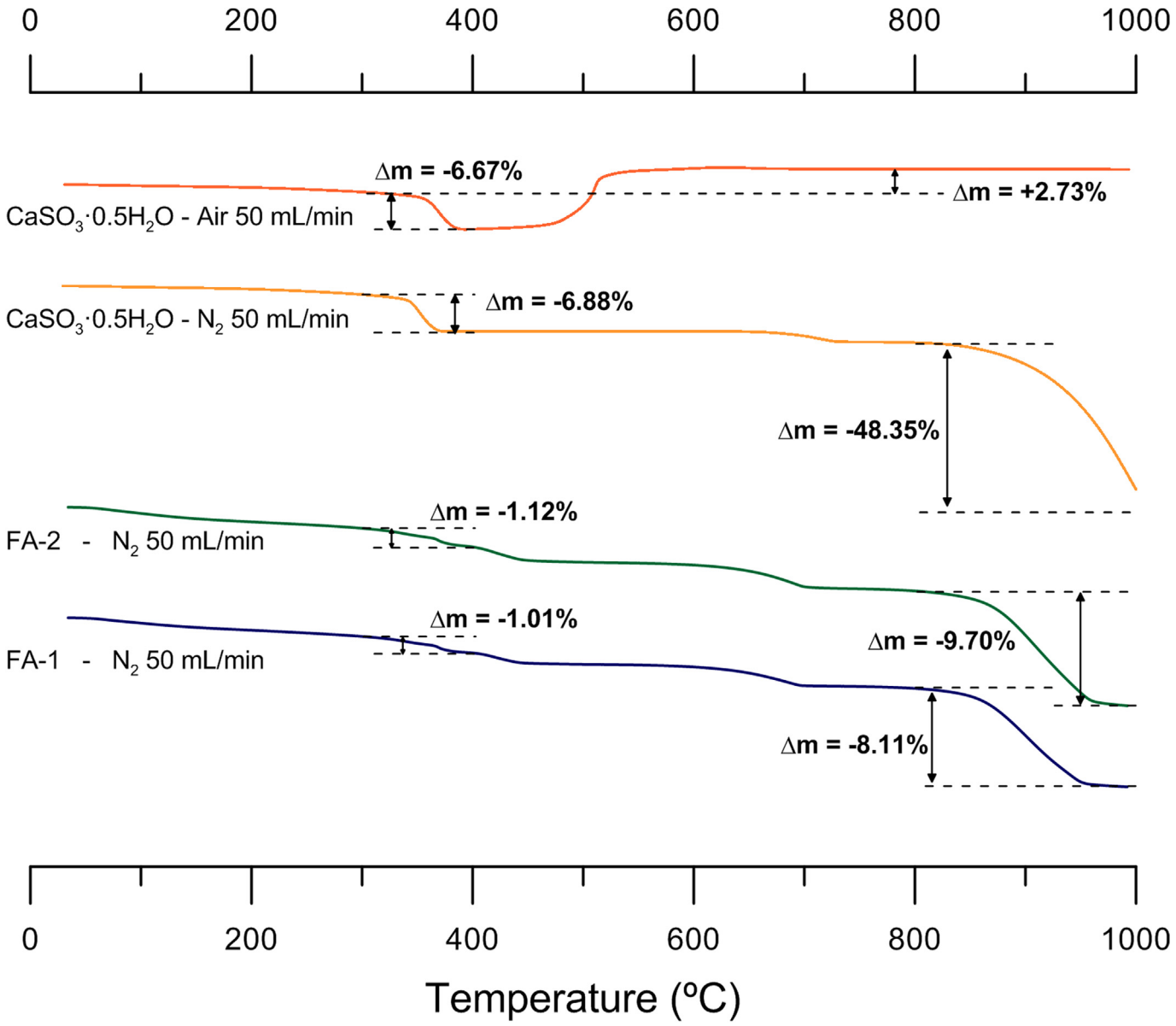

Fig. 4. TGA mass loss curves for FA-1, FA-2 in N_2 atmosphere and pure hannebachite samples in N_2 and air atmosphere.

been observed previously [21,36], and has been attributed to the formation of a lower quality (higher porosity) C-S-H due to the extreme acceleration of the C_3S reaction typically induced by $CaCl_2$.

5.4. Isothermal calorimetry

To better appreciate the effects of the accelerating strategies on hydration kinetics, results are presented separately for each of the different methodologies studied. Heat flow results are presented normalized by OPC content to observe acceleration/retardation and activation/suppression of the reaction kinetics of cement by the inclusion of the FA. On the other hand, total heat is presented normalized by initial volume of water, as it has been shown that this normalization can be linearly correlated with compressive strength [54].

5.4.1. Physical acceleration: limestone powder

Heat flow and total heat release curves for the LS and FLS blended systems are presented in Fig. 7, along with the FA-1 and FA-2 results to be considered for comparison. FA retardation extends the induction period and reduces the rate of the OPC silicates' hydration, which is observed as a height reduction in the first peak (Fig. 7a). Systems containing LS powder exhibit amplification of the silicates reaction, while some acceleration is also observed. This is attributed to the limestone grains providing more surface and stimulating the nucleation of C-S-H [55]. FLS additions enhance this acceleration effect, in good agreement with the setting time results and the higher SSA of this material compared to the original LS. Total heat release shows that samples containing FLS exhibit higher heat release per unit volume of water up to 24 h of hydration (Fig. 7b), suggesting a higher strength of these mixtures at 1 d. However, the difference between FLS and LS disappears by 3 d, in general agreement with the observations from compressive strength tests at 3 d and 7 d, where no significant differences were observed between the LS and FLS mixtures.

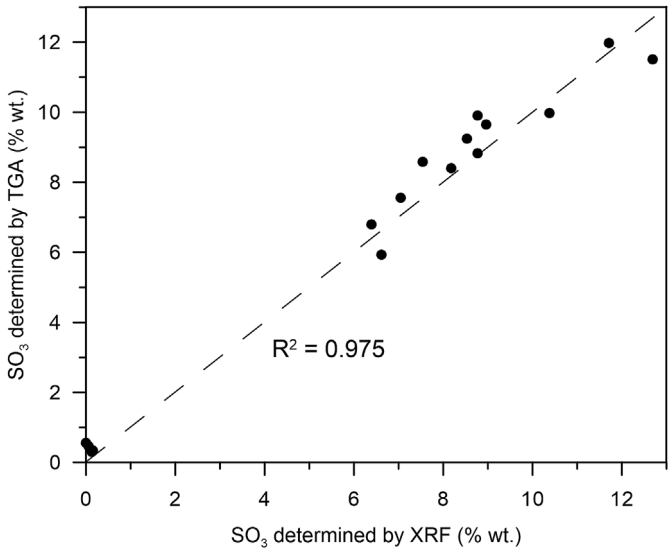

Fig. 5. SO_3 content determined by XRF analysis versus SO_3 content determined by TGA analysis using Eq. (1).

5.4.2. Chemical acceleration: calcium chloride

Isothermal calorimetry results for systems containing $CaCl_2$ are presented in Fig. 8. Additions of 2% or 3% $CaCl_2$ produce a strong acceleration of hydration, in agreement with the initial setting time results discussed previously. A single peak is observed in these systems, as the heavily accelerated C_3S reaction overwhelms the second (smaller) aluminates peak (Fig. 8a). This is due to the stimulation of the C_3S reaction provided by $CaCl_2$ [50], leading to an increase of the rate of formation of inner product C-S-H [56]. These results are in general agreement with previous observations on mortar systems with a similar composition [21]. The heat release for calcium chloride systems is higher during the first 48 h compared to the reference FA-1 and FA-2 systems (Fig. 8b). Thus, higher compressive strengths could be expected during this period. In addition, the difference disappears during the third day of hydration, which again is consistent with the fact that no significant differences in compressive strengths of mixtures containing calcium chloride and the other systems were observed at 3 d, and where $CaCl_2$ systems had lower strengths at 7 d. While the $CaCl_2$ acceleration mechanism is still not fully understood, this behavior may be caused by a quick filling of the capillary pores with a more porous C-S-H having loosely incorporated water [36], which would reduce the space available to form additional hydration products at later ages.

5.4.3. Fly ash pre-washing

Isothermal calorimetry measurements on systems containing pre-washed FA are presented in Fig. 9. The effect on hydration kinetics is similar to that observed when using LS or FLS. The hybrid system containing pre-washed FA and FLS exhibits an even greater acceleration, in agreement with the additional shortening of setting times. Heat release of pre-washed FA systems is higher than those of FA-1 and FA-2 during the first 36 h of hydration, but similar at 3 d. This suggests that while the pre-washing may reduce the initial setting retardation effect of FA, after the formation of the first percolated structure, the strength development is dominated by

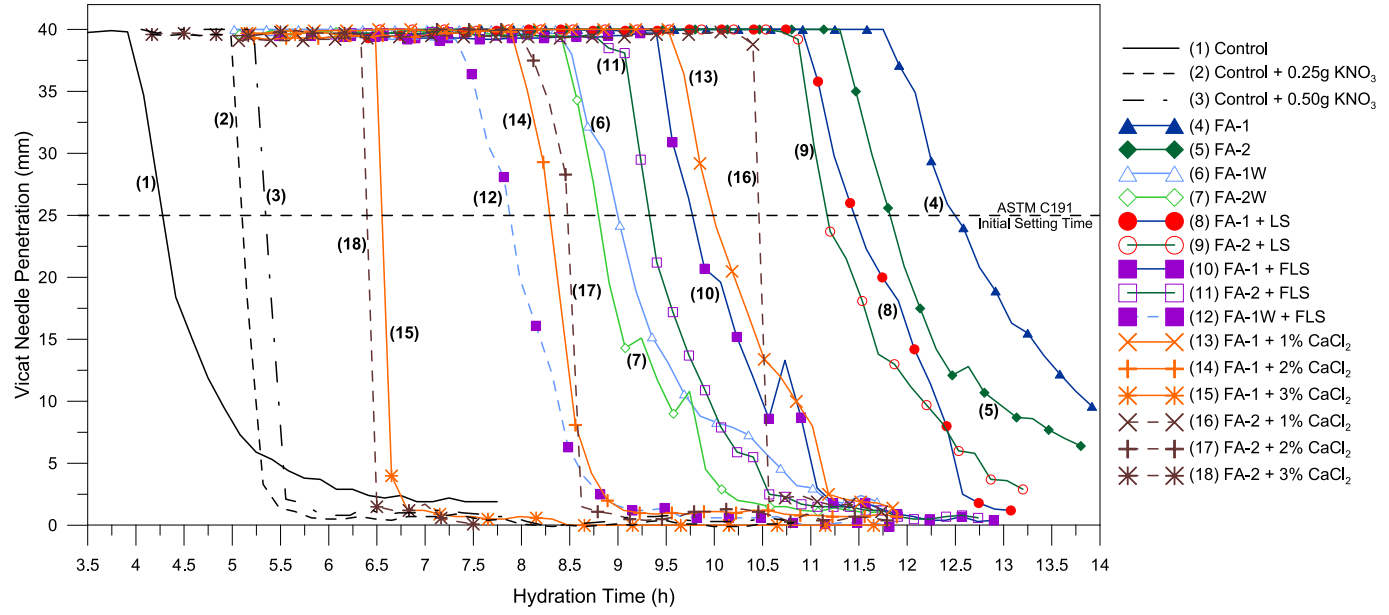

Fig. 6. Setting time (Vicat needle) results for mixtures studied. Initial setting time can be found for each mixture as the intersection of the 25 mm penetration dashed line and the measured curve.

Table 3
Compressive strength results of cement paste samples at 3 d and 7 d (STD indicates standard deviation).

MIX ID	Control	FA-1	FA-2	FA-1W	FA-2W	FA-1 +LS	FA-2 +LS	FA-1 +FLS	FA-2 +FLS	FA-1 + 2%$CaCl_2$	FA-2 + 2%$CaCl_2$	FA-1 + 3%$CaCl_2$	FA-2 + 3%$CaCl_2$
3d strength (MPa)	37.85	16.31	15.66	17.84	17.93	18.55	19.04	17.97	18.19	18.19	17.63	18.15	17.63
3d STD (MPa)	1.08	1.03	0.84	0.50	0.91	0.97	0.53	0.66	0.25	0.25	0.81	0.62	0.52
7d strength (MPa)	48.55	26.96	29.26	30.96	30.46	31.91	30.53	31.77	31.48	30.72	29.41	29.87	28.17
7d STD (MPa)	2.61	0.98	0.55	1.89	1.05	1.95	1.88	0.32	0.89	0.61	1.51	1.41	0.43

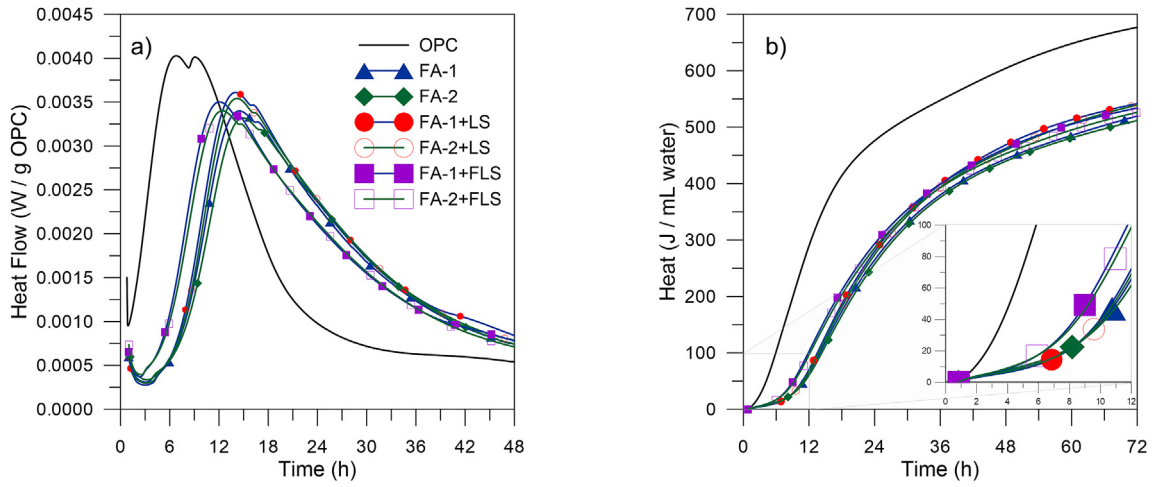

Fig. 7. Isothermal calorimetry results for mixtures incorporating HSFA and limestone powder, a) heat flow versus time and b) heat release per unit volume of water.

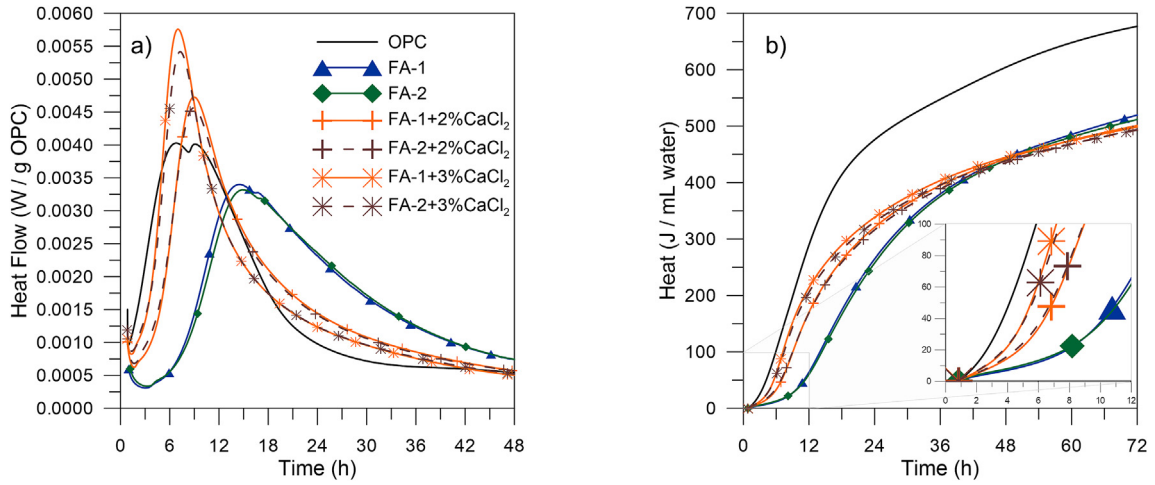

Fig. 8. Isothermal calorimetry results for mixtures incorporating HSFA and calcium chloride, a) heat flow versus time and b) heat release per unit volume of water.

the same hydration reactions as those present in the non-treated systems.

In order to contrast the kinetic data gathered by isothermal calorimetry with setting time measurements, two hydration time markers were compared with setting times. First, the time required for a total heat release of 50 J/mL water was selected, is it was

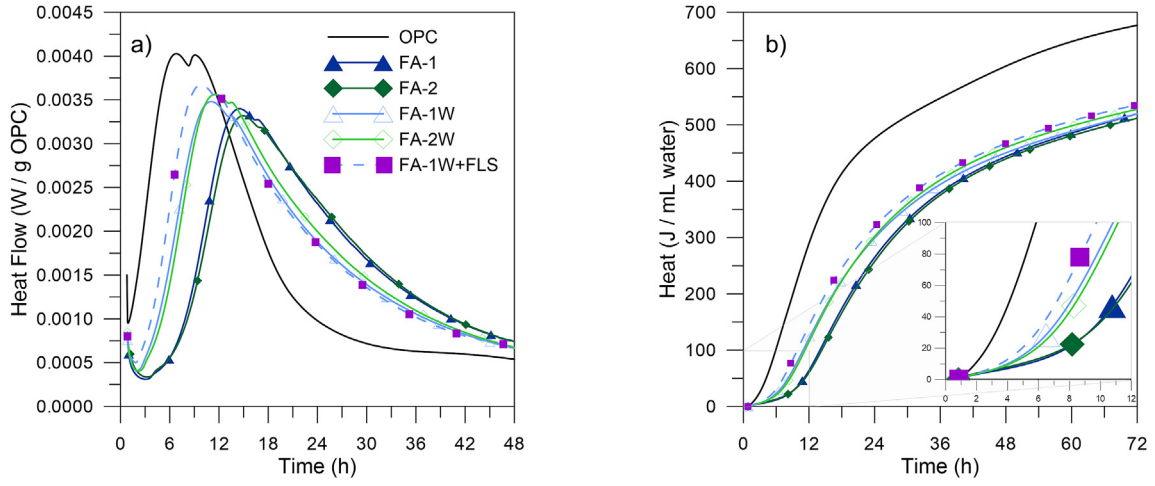

Fig. 9. Isothermal calorimetry results for mixtures incorporating HSFA and pre-washed ashes, a) heat flow versus time and b) heat release per unit volume of water.

observed to be a good indicator of the hydration during the first 12 h for all the systems studied. As this selection was based on the data of the systems studied and may be arbitrary to be extended to different FAs, the time of the first (silicate) peak was also used. Both comparisons are shown on Fig. 10. As observed, both markers correlate linearly with setting times. Thus, the effect of the acceleration strategies on setting can be assessed using data gathered from isothermal calorimetry, if the same *w/s* ratio is used among them. This also shows that, for a given *w/s*, setting time is a function of the initial rate of reaction of silicates and the time elapsed before the acceleration of the silicates' reaction starts (length of the induction period).

5.5. SEM microscopy

5.5.1. High resolution SEM

Micrographs of a non-HSFA sample that was analyzed as a reference, and both FA-1 and FA-2 used in this study are shown in Fig. 11. It can be seen that the reference FA sample (Fig. 11 top) is mainly composed of the typical spherical particles, surrounded by irregularly shaped crystals of quartz. The surface of the spheres appears free of large impurities and the particles remain isolated from one another, which explains the pseudo-fluid aspect of this FA when manipulated.

The microstructural morphology of FA-1 and FA-2 (Fig. 11 middle and bottom, respectively) differs significantly from the one observed in the reference FA. In this case, spherical particles appear surrounded and highly intermixed with an irregularly shaped phase. EDS analysis identified these regions as a mixture of hannebachite, the calcium sulfite compound identified in the HSFA samples, calcite, and portlandite. While this material is observed in all the of the FA images, the spherical particles are still identifiable, suggesting a strong intermixing of the two solid phases but not a chemical combination of them. This is consistent with the powders' bimodal PSD (Fig. 2). By observation, the population of finer particles is associated with the irregular shaped particles surrounding the second and larger population of spherical FA particles.

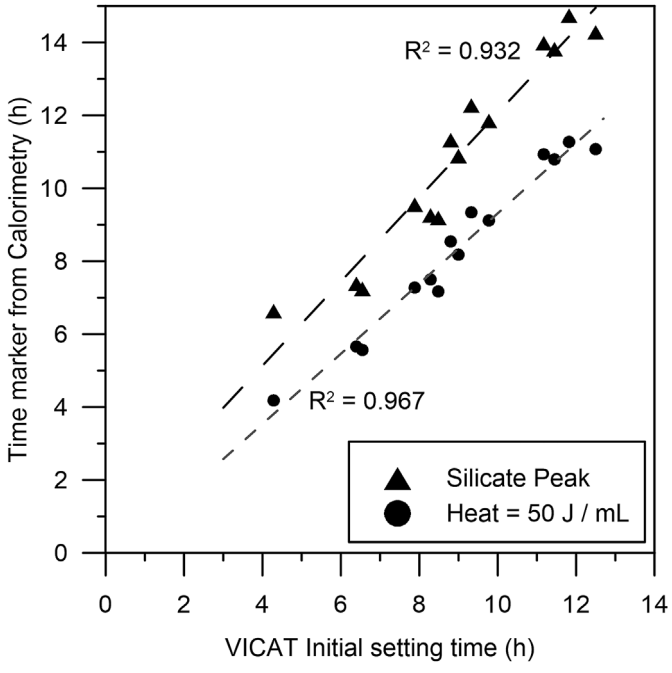

Fig. 10. Comparison between Vicat setting time and relevant hydration time markers determined from isothermal calorimetry.

5.5.2. EDS mapping

Using the EDS data collected from the polished sections of the reference FA and FA-2, ternary frequency plots were constructed using the methodology proposed in Ref. [6]. This representation proved to be more useful than raw elemental maps to identify populations of chemical composition present in the different samples analyzed, and also to identify differences in the composition of the amorphous fraction of FA, which cannot be studied by XRD. The classical Al-Si-Ca diagram was computed, and an additional S-Mg-Ca plot was included to assess the nature of the SO_3-rich phase.

Fig. 12 shows the ternary frequency plots for the reference non-SO_3 rich FA (top) and FA-2 (bottom), which is taken as an example of both HSFAs studied (as the same trends were observed between them). It can be observed that the composition of the amorphous phase in the reference FA falls in the region of silicate and alumino-silicate regions, as defined in Ref. [6]. No compositional populations towards calcium rich phases are observed, which is consistent with the chemical composition of a Class F fly ash [2], which was confirmed as well by XRF under the requirements of ASTM C618 [26]. The S-Mg-Ca ternary diagram of this sample shows that the sulfur-rich regions are not associated with cations such as calcium or magnesium. Therefore, it is most likely to be attributed to sulfur present in unburnt coal particles present inside the FA.

In the case of FA-2 (Fig. 12 bottom), the primary composition is still located in the alumino-silicate region. This reinforces the observation made based on HR-SEM micrographs, where it was observed that the two solid phases are intermixed but not combined. Thus, the population corresponding to the spherical FA particles remains located in the same region of the Al-Si-Ca ternary diagram. In this case, particles moving towards a high calcium content are also observed, being consistent with the expected composition of a Class C fly ash [2]. These particles correspond to hannebachite, calcite and portlandite. The S-Mg-Ca ternary diagram shows a large population of particles of calcium-sulfur intermixed composition. This is consistent with the mineralogical nature of the SO_3-rich phase identified by XRD in this sample (hannebachite).

6. Conclusions

This paper is part of a study focused on assessing the feasibility to incorporate fly ashes with high levels of SO_3 impurities in cement-based materials. In particular, this study focused on the setting retardation observed with these fly ashes, and the different acceleration strategies that were explored. It was shown that the SO_3-rich compounds in the fly ashes do not correspond to calcium sulfate (gypsum), but rather to a reduced form of this compound (calcium sulfite, or hannebachite). Therefore, new opportunities for research on these materials are conceived, because the solubility of calcium sulfite is much lower than that of calcium sulfate, and the reactions between this compound and cement phases have not been previously described.

Based on the results of this study, it can be concluded:

1. The SO_3-rich phase (calcium sulfite) is present as separate and smaller particles that are distinct from the larger FA spherical particles in HSFAs, suggesting that calcium sulfite precipitates in a different stage of the combustion process. These two particle populations are intermixed to give the powder a bimodal particle size distribution. This could open a feasible scenario for the application of particle separation techniques such as sedimentation and air separation to exclude the SO_3-rich phase.

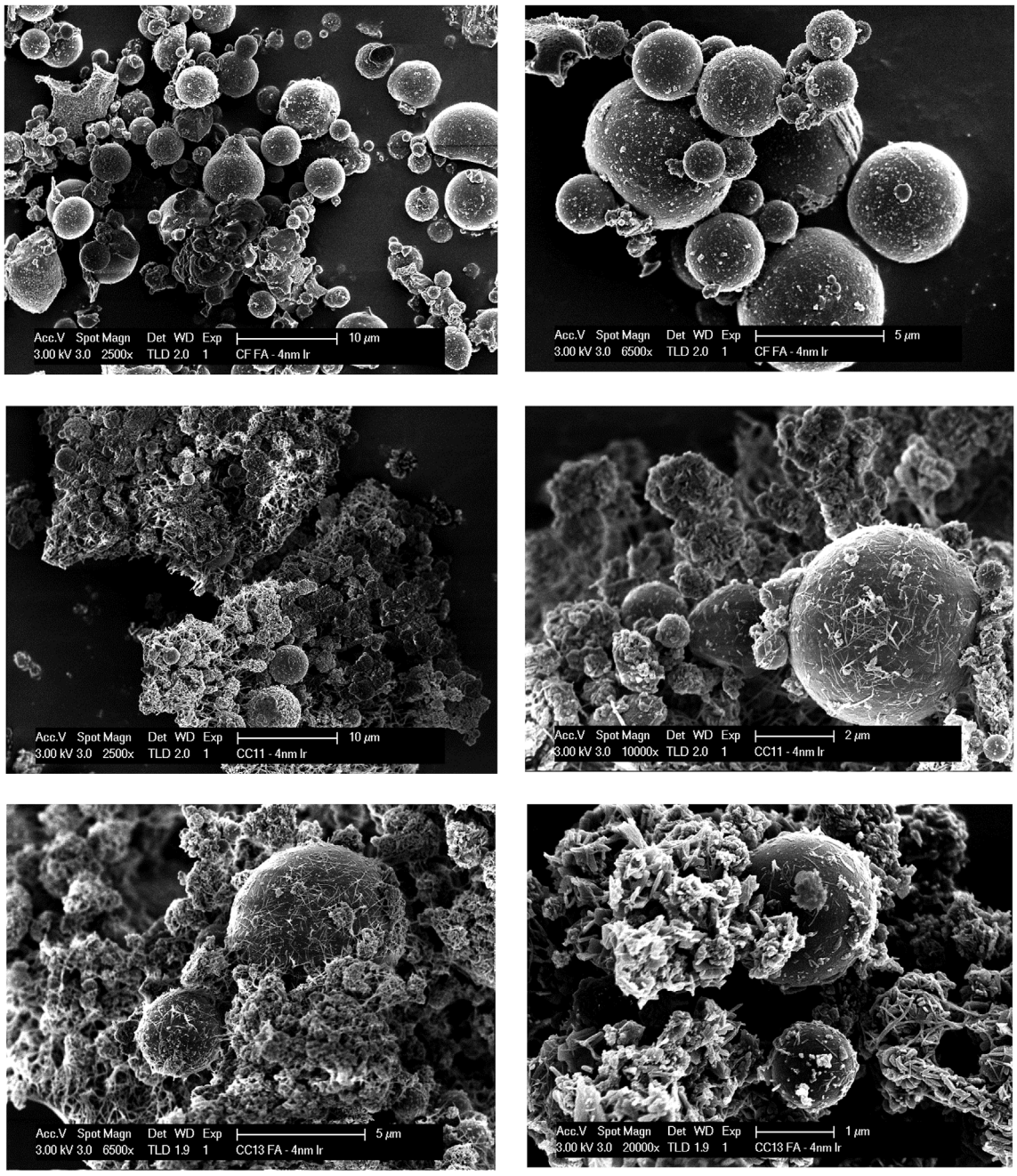

Fig. 11. HR-SEM micrographs of non-SO_3 rich reference FA (top), FA-1 (middle) and FA-2 (bottom) samples.

2. Thermogravimetric analysis proved to be a reliable tool to estimate the SO_3 content of HSFA. It offers a faster and almost preparation-free alternative to the traditional XRF analysis. Furthermore, performing the analysis in the recommended temperature range of 300 °C—400 °C may allow one to obtain results from a simple mass balance and furnace setup, equipment available in almost any characterization laboratory, and presents a new opportunity for field assessment of HSFA.
3. Limestone powder, calcium chloride, and fly ash pre-washing all proved to be somewhat effective in accelerating the initial setting time. Among these strategies, the combination of limestone powder and fly-ash pre-washing may offer a sustainable and inexpensive methodology in compliance with chloride restrictions for reinforced structures. Nevertheless, when allowed, calcium chloride may also be employed as an effective setting accelerator for these systems.
4. Isothermal calorimetry showed that the retardation in setting is explained by an extension of the induction period in systems containing HSFA. Limestone powder and fly-ash pre-washing accelerate the setting of the mixtures by shortening this extended induction period, while the effect of calcium chloride appears to be dominated by the activation of the silicates' reaction, observed as an amplification and acceleration of the first hydration peak.

Studies concerning phase assemblage, hydration kinetics, volumetric stability and durability are considered as future stages of this research project and are currently in ongoing development.

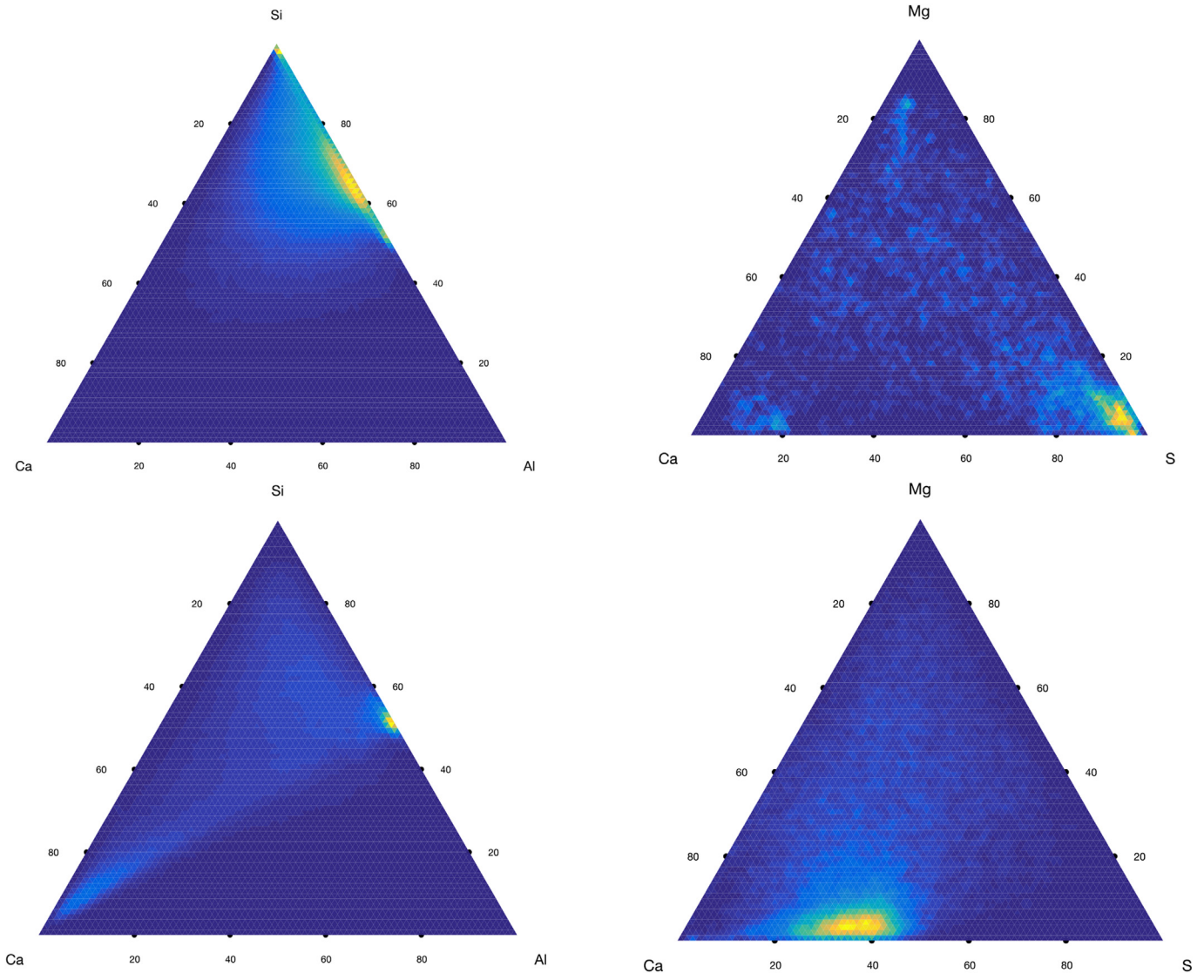

Fig. 12. Al-Si-Ca and S-Mg-Ca ternary frequency plots of a non-SO_3 rich FA (top) and FA-2 (HSFA, bottom) used in this study. The scale on each diagram is adjusted so that the lower value is represented by dark blue and the highest by yellow. (For interpretation of the references to colour in this figure legend, the reader is referred to the Web version of this article.)

These findings will be presented in forthcoming publications by the research team.

Acknowledgments

The authors gratefully acknowledge support provided by Prof. Karen Scrivener from the Construction Materials Laboratory (LMC) at École Polytechnique Fédérale de Lausanne, for facilitating access to the SEMs used in this study. Also, the authors acknowledge Mr. Rajiv Vaswani for his support in conducting the setting time tests presented in this paper. Finally, the authors would like to acknowledge the financial support provided by CONICYT through its project Fondecyt Nº1160804.

References

[1] M. Schneider, M. Romer, M. Tschudin, H. Bolio, Sustainable cement production—present and future, Cement Concr. Res. 41 (2011) 642–650, https://doi.org/10.1016/j.cemconres.2011.03.019.
[2] B. Lothenbach, K. Scrivener, R.D. Hooton, Supplementary cementitious materials, Cement Concr. Res. 41 (2011) 1244–1256, https://doi.org/10.1016/j.cemconres.2010.12.001.
[3] N. Jain, Effect of nonpozzolanic and pozzolanic mineral admixtures on the hydration behavior of ordinary Portland cement, Construct. Build. Mater. 27 (2012) 39–44, https://doi.org/10.1016/j.conbuildmat.2011.08.006.
[4] E. Karim, K. El-Hadj, B. Abdelkader, B. Rachid, Analysis of mortar long-term strength with supplementary cementitious materials cured at different temperatures, ACI Mater. J. (2010) 323–331.
[5] P. Mehta, Durability - critical issues for the future, Concr. Int. 19 (1997) 69–76.
[6] P.T. Durdzinski, C.F. Dunant, M. Ben Haha, K.L. Scrivener, A new quantification method based on SEM-EDS to assess fly ash composition and study the reaction of its individual components in hydrating cement paste, Cement Concr. Res. 73 (2015) 111–122, https://doi.org/10.1016/j.cemconres.2015.02.008.
[7] V.G. Papadakis, S. Tsimas, Supplementary cementing materials in concrete Part I : efficiency and design, Cement Concr. Res. 32 (2002) 1525–1532.
[8] A. Schöler, B. Lothenbach, F. Winnefeld, M. Zajac, Hydration of quaternary Portland cement blends containing blast-furnace slag, siliceous fly ash and limestone powder, Cement Concr. Compos. 55 (2015) 374–382, https://doi.org/10.1016/j.cemconcomp.2014.10.001.
[9] D.P. Bentz, C.F. Ferraris, Rheology and setting of high volume fly ash mixtures, Cement Concr. Compos. 32 (2010) 265–270, https://doi.org/10.1016/j.cemconcomp.2010.01.008.
[10] D.P. Bentz, Activation energies of high-volume fly ash ternary blends: hydration and setting, Cement Concr. Compos. 53 (2014) 214–223, https://doi.org/10.1016/j.cemconcomp.2014.06.018.
[11] I. De la Varga, J. Castro, D.P. Bentz, F. Zunino, J. Weiss, Evaluating the hydration

of high volume fly ash mixtures using chemically inert fillers, Construct. Build. Mater. 161 (2018) 221–228, https://doi.org/10.1016/j.conbuildmat.2017.11.132.
[12] V. Malhotra, P. Mehta, High-performance, high-volume fly ash concrete for building durable and sustainable structures, 4th editio, supplementary cementing materials for sustainable development, inc., Ottawa, 2012.
[13] D.P. Bentz, C.F. Ferraris, K. Snyder, Best Practices Guide for High-volume Fly Ash Concretes: Assuring Properties and Performance, NIST Technical Note 1812, U.S. Department of Commerce, 2013.
[14] S.J. Choi, S.S. Lee, P.J.M. Monteiro, M. Asce, Effect of fly ash fineness on temperature rise, setting, and strength development of mortar, ASCE J. Mater. Civ. Eng 24 (2012) 499–505, https://doi.org/10.1061/(ASCE)MT.1943-5533.0000411.
[15] K. De Weerdt, K.O. Kjellsen, E. Sellevold, H. Justnes, Synergy between fly ash and limestone powder in ternary cements, Cement Concr. Compos. 33 (2011) 30–38, https://doi.org/10.1016/j.cemconcomp.2010.09.006.
[16] K. De Weerdt, M. Ben Haha, G. Le Saout, K.O. Kjellsen, H. Justnes, B. Lothenbach, Hydration mechanisms of ternary Portland cements containing limestone powder and fly ash, Cement Concr. Res. 41 (2011) 279–291, https://doi.org/10.1016/j.cemconres.2010.11.014.
[17] P.T. Durdziński, M. Ben Haha, M. Zajac, K.L. Scrivener, Phase assemblage of composite cements, Cement Concr. Res. 99 (2017) 172–182, https://doi.org/10.1016/j.cemconres.2017.05.009.
[18] P. Van den Heede, E. Gruyaert, N. De Belie, Transport properties of high-volume fly ash concrete: capillary water sorption, water sorption under vacuum and gas permeability, Cement Concr. Compos. 32 (2010) 749–756, https://doi.org/10.1016/j.cemconcomp.2010.08.006.
[19] I. De La Varga, R.P. Spragg, C. Di Bella, J. Castro, D.P. Bentz, J. Weiss, Fluid transport in high volume fly ash mixtures with and without internal curing, Cement Concr. Compos. 45 (2014) 102–110, https://doi.org/10.1016/j.cemconcomp.2013.09.017.
[20] V.M. Malhotra, M.H. Zhang, G.H. Leaman, Long-term performance of steel reinforcing bars in portland cement concrete and concrete incorporating moderate and high volumes of ASTM Class F fly ash, ACI Mater. J. 97 (2000) 409–417.
[21] D.P. Bentz, F. Zunino, D. Lootens, Chemical versus physical acceleration of cement hydration, Concr. Int. 38 (2016) 37–44.
[22] D.P. Bentz, T. Sato, I. De La Varga, W.J. Weiss, Fine limestone additions to regulate setting in high volume fly ash mixtures, Cement Concr. Compos. 34 (2012) 11–17, https://doi.org/10.1016/j.cemconcomp.2011.09.004.
[23] F. Scala, M. D'Ascenzo, A. Lancia, Modeling flue gas desulfurization by spray-dry absorption, Separ. Purif. Technol. 34 (2004) 143–153, https://doi.org/10.1016/S1383-5866(03)00188-6.
[24] J.M. Bigham, D. a Kost, R.C. Stehouwer, J.H. Beeghly, R. Fowler, S.J. Traina, et al., Mineralogical and engineering characteristics of dry flue gas desulfurization products, Fuel 84 (2005) 1839–1848, https://doi.org/10.1016/j.fuel.2005.03.018.
[25] G.F. Martha de Souza (Ed.), Thermal Power Plant Performance Analysis, Springer, London, 2012.
[26] ASTM C618, Standard Specification for Coal Fly Ash and Raw or Calcined Natural Pozzolan for Use in Concrete, 2008.
[27] T. Ikumi, S.H.P. Cavalaro, I. Segura, A. Aguado, Alternative methodology to consider damage and expansions in external sulfate attack modeling, Cement Concr. Res. 63 (2014) 105–116, https://doi.org/10.1016/j.cemconres.2014.05.011.
[28] H. Taylor, C. Famy, K. Scrivener, Delayed ettringite formation, Cement Concr. Res. 31 (2001) 683–693, https://doi.org/10.1016/S0008-8846(01)00466-5.
[29] C. Li, H. Zhong, S. Wang, J. Xue, H. Wang, Reaction process and mechanism analysis for CaS generation in the process of reductive decomposition of CaSO3 with coal, J. Taiwan Inst. Chem. Eng 50 (2015) 173–181, https://doi.org/10.1016/j.jtice.2014.12.032.
[30] F.F. Hill, J. Zank, Flue gas desulphurization by spray dry absorption, Chem. Eng. Process. Process Intensif 39 (2000) 45–52, https://doi.org/10.1016/S0255-2701(99)00077-X.
[31] Y. Zhou, X. Zhu, J. Peng, Y. Liu, D. Zhang, M. Zhang, The effect of hydrogen peroxide solution on SO2 removal in the semidry flue gas desulfurization process, J. Hazard Mater. 170 (2009) 436–442, https://doi.org/10.1016/j.jhazmat.2009.04.075.
[32] P. Mehta, P. Monteiro, Concrete: Microstructure, Properties, and Materials, third ed., McGraw-Hill Professional, New York, 2005.
[33] W. Lerch, The influence of gypsum on the hydration and properties of portland cement pastes, Proc. Am. Soc. Test. Mater. 46 (1946) 1252–1291.
[34] J.T. Riley, M. Marsh, D. Lawrenz, Analysis of FGD solids with a macro TGA system, J. Test. Eval. 45 (2016), https://doi.org/10.1520/JTE20160079.
[35] K. Scrivener, R. Snellings, B. Lothenbach (Eds.), A Practical Guide to Microstructural Analysis of Cementitious Materials, CRC Press, 2016, https://doi.org/10.7693/wl20150205.
[36] V.K. Peterson, M.C.G. Juenger, Hydration of tricalcium silicate: effects of CaCl2 and sucrose on reaction kinetics and product formation, Chem. Mater. 18 (2006) 5798–5804, https://doi.org/10.1021/cm061724y.
[37] D.A. Silva, J. Cheung, P. Sandberg, L. Roberts, D. Subramanian, J. Gallagher, et al., Suppression of Antagonistic Hydration Reactions in Blended Cements, US008518176B2, 2013.
[38] D.P. Bentz, C.F. Ferraris, S.Z. Jones, D. Lootens, F. Zunino, Limestone and Silica Powder Replacements for cement: early-age performance, Cement Concr. Compos. 78 (2017) 43–56, https://doi.org/10.1016/j.cemconcomp.2017.01.001.
[39] P. Lawrence, M. Cyr, E. Ringot, Mineral admixtures in mortars effect of type, amount and fineness of fine constituents on compressive strength, Cement Concr. Res. 35 (2005) 1092–1105, https://doi.org/10.1016/j.cemconres.2004.07.004.
[40] F. Zunino, M. Lopez, Decoupling the physical and chemical effects of supplementary cementitious materials on strength and permeability: a multi-level approach, Cement Concr. Compos. 65 (2016) 19–28, https://doi.org/10.1016/j.cemconcomp.2015.10.003.
[41] F. Zunino, M. Lopez, A methodology for assessing the chemical and physical potential of industrially sourced rice husk ash on strength development and early-age hydration of cement paste, Construct. Build. Mater. 149 (2017) 869–881.
[42] ACI 318M, Building Code Requirements for Structural Concrete, 2011.
[43] ASTM C191, Standard Test Methods for Time of Setting of Hydraulic Cement by Vicat Needle, 2008, https://doi.org/10.1520/C0191-08.2.
[44] L. Schropfer, Strukturelle untersuchungen an CaSO3·1/2H2O, zeitschrift Fur anorg, Und Allg. Chemie 401 (1973) 1–14.
[45] G. Hentschel, E. Tillmanns, W. Hofmeister, Hannebachite, natural calcium-sulfite hemihydrate, CaSO3·1/2H2O, Neues Jahrb. Für Mineral (1985) 241–250.
[46] IUPAC Solubility Data, Calcium Sulfite Solubility, 1986. http://srdata.nist.gov/solubility/IUPAC/SDS-26/SDS-26.html.
[47] American Chemical Society, Reagents Chemicals: Specifications and Procedures, Oxford University Press, 2006.
[48] H.A. Papazian, P.J. Pizzolato, J. Peng, Observations of the thermal decomposition of some dithionates and sulfites, Thermochim. Acta 5 (1972) 147–152.
[49] S.E. Bogushevich, G.N. Lysenko, Spectroscopic study of calcium sulfite thermolysis, Russ. J. Inorg. Chem. 54 (2009) 618–623, https://doi.org/10.1134/S0036023609040196.
[50] B.A.M. Rosenberg, T.H.E.E. Of, Study of the mechanism through which calcium chloride accelerates the set of portland cement, J. Am. Concr. Inst. 61 (1964) 1261–1268.
[51] D.P. Bentz, P.E. Stutzman, F. Zunino, Low-temperature curing strength enhancement in cement-based materials containing limestone powder, Mater. Struct. 50 (2017).
[52] A. Ipavec, R. Gabrovšek, T. Vuk, V. Kaučič, J. MačEk, A. Meden, Carboaluminate phases formation during the hydration of calcite-containing Portland cement, J. Am. Ceram. Soc. 94 (2011) 1238–1242, https://doi.org/10.1111/j.1551-2916.2010.04201.x.
[53] T. Matschei, B. Lothenbach, F.P. Glasser, Thermodynamic properties of Portland cement hydrates in the system CaO-Al2O3-SiO2-CaSO4-CaCO3-H2O, Cement Concr. Res. 37 (2007) 1379–1410, https://doi.org/10.1016/j.cemconres.2007.06.002.
[54] D.P. Bentz, T. Barrett, I. De la Varga, W.J. Weiss, Relating compressive strength to heat release in mortars, Adv. Civ. Eng. Mater 1 (2012) 1–16, https://doi.org/10.1520/ACEM20120002.
[55] E. Berodier, K. Scrivener, Understanding the filler effect on the nucleation and growth of C-S-H, J. Am. Ceram. Soc. 97 (2014) 3764–3773, https://doi.org/10.1111/jace.13177.
[56] M.C.G. Juenger, P.J.M. Monteiro, E.M. Gartner, G.P. Denbeaux, A soft X-ray microscope investigation into the effects of calcium chloride on tricalcium silicate hydration, Cement Concr. Res. 35 (2005) 19–25, https://doi.org/10.1016/j.cemconres.2004.05.016.